PCCP

Accepted Manuscript

This is an *Accepted Manuscript*, which has been through the Royal Society of Chemistry peer review process and has been accepted for publication.

Accepted Manuscripts are published online shortly after acceptance, before technical editing, formatting and proof reading. Using this free service, authors can make their results available to the community, in citable form, before we publish the edited article. We will replace this *Accepted Manuscript* with the edited and formatted *Advance Article* as soon as it is available.

You can find more information about *Accepted Manuscripts* in the Information for Authors.

Please note that technical editing may introduce minor changes to the text and/or graphics, which may alter content. The journal's standard Terms & Conditions and the Ethical guidelines still apply. In no event shall the Royal Society of Chemistry be held responsible for any errors or omissions in this *Accepted Manuscript* or any consequences arising from the use of any information it contains.

ROYAL SOCIETY OF CHEMISTRY

www.rsc.org/pccp

Journal Name

ARTICLE

Can betaine pyridinium derivatives be used to control the photoejection of cation?

Received 00th January 20xx,
Accepted 00th January 20xx

DOI: 10.1039/x0xx00000x

www.rsc.org/

S. Aloïse*, [a] Y. Ruan, [b] I. Hamdi, [a] A. K. Tiwari, [a] G. Buntinx, [a] C. Azarias, [c,d] A. Perrier, [c,d] and I. Leray*[b]

Using a combination of advanced DFT/TDDFT calculations together with ultrafast and stationary spectroscopies we have investigated the photochemistry and cationic complexation ability of 1-pyridinio-benzimidazolate (PyB) and analogs substituted by an 15-aza-5-crown (PyB-Aza) or dimethyl-amino groups (PyB-DiMe). Focusing on PyB-Aza, the first aim was to assess the competitive complexation of the imidazole bridge vs the macrocycle. In acetonitrile, it was found by absorption and emission that the imidazole moiety bind efficiently through lateral electrostatic interaction of high charge density cations and especially Ca^{2+} to form a 1:1, metal:ligand (M:L) complex. Modulation of the complexation toward para substitution of the phenyl ring with a donor group is reported with values ranging from log K=3.4 to 6.8. Complexation values are properly predicted by DFT calculations. From a photochemical point of view, for the same series, the trend is parallel to the rate of the photo-release process found to be less than 200 femtosecond (fs), fastest photorelease characteristic time never reported so far. Unlike photoinduced charge transfer molecules linked with aza-crown, the mechanism appears simpler with no participation of loose complex due to macrocavity effect. Relaxations mechanisms after cation ejections are discussed as well. Finally, even if for the PyB-Aza molecule, any photoinduced translocation of cation is reported between two complexation sites, a discussion about the use of betaine pyridinium as a molecular brick of smart manipulating cation system is initiated.

Introduction

The complexing and precise spatiotemporal release of bioactive compounds are becoming very important in the field of supramolecular chemistry, life science and nanomedicine. A particular focus has been given on the development of chemical cages for metal ions, such as calcium ions (Ca^{2+}) because of its biological importance. Ca^{2+} has been studied extensively in muscle contraction, cell signaling, gene regulation, thrombosis, wound healing, and cell death.[1]

In the race to achieve an actual control on bioactive cations, the use of light is an attractive way because it is non-invasive and readily delivered with high spatial and temporal precision.[2] Recent examples of drug delivery systems induced by light have been successfully reported[3] even if the lack of reversibility was still a major drawback to overpass. Indeed, after photorelease, the host molecule becomes structurally different and thus unable to cage again an ion.[4] A solution consists in using photo-induced charge transfer (PCT) molecules coupled with complexing agent typically aza-crown for which the cation delivery process stops with the end of illumination. Indeed, PCT leads to the positive polarization of heteroatom of the macrocycle, resulting in the Coulombic repulsion between the heteroatom and metal cation initially present in the cavity. Such system has been proposed based on azacrown-subsituted $[(bpy)Re(CO)_3L]^+$ complex,[5] flavonol derivatives[6], benzylhydrazone[7] and pyridyl oxadiazole.[8] Additional refinement can be obtained using fluorophore as PCT moiety which allow tracking the cation photo-release through stationary and time resolved spectroscopy. For example, the study of merocyanine linked to aza-crown moiety (DCM-crown) has shown that the cation photoejection mechanism is a multi-step process occurring within hundred picoseconds (ps).[9] Apart from one recent novel proposition

[a] Univ.Lille, CNRS, UMR 8516, LASIR, Laboratoire de Spectrochimie Infrarouge et Raman, F59 000 Lille, France.
[b] ENS-CACHAN PPSM-CNRS 8531, 61, av. du Président Wilson, 94235 Cachan, France.
[c] ITODYS, UMR CNRS 7086, Université Paris Diderot, Sorbonne Paris Cité, 15 rue Jean Antoine de Baif, 75205 Paris Cedex 13, France
[d] Chimie Paris Tech, PSL Research University, CNRS, Institut de Recherche de Chimie Paris (IRCP), F-75005 Paris, France.

* Corresponding authors: stephane.aloise@univ-lille1.fr; icmleray@ppsm.ens-cachan.fr

Electronic Supplementary Information (ESI) available: [additional Ca^{2+} titration using absorption and fluorescence; Transient data for PyB-DiMe; scheme for logK calculations; Solvatochromic and Kamlet-Taft study for PyB-Aza]. See DOI: 10.1039/x0xx00000x

Physical Chemistry Chemical Physics Accepted Manuscript

Please do not adjust margins

based on calixarene double cages[10], the molecular engineering dealing with the spatio-temporal control of cations is always requesting novel PCT chromophores to enlarge the possible combination of more and more elaborated system.

In this context, betaine pyridinium molecules are interesting entities because they can interact with cations. Reichardt et al. in 1992 reported drastic modification of UV-Visible spectra of the well-known solvatochromic probe betaine-30 induced by the presence of ion, the so called halochromic effect.[11] It was rationalized in terms of electrostatic interaction between negative phenolate oxygen and the cation. Cation selectivity has been reported using appropriate crown-ether substitution.[11-12] In the same way, focusing on neighbouring benzimidazole compounds, Kumar et al. reported multiple ionophore optical probe able to screen various metal ions.[8] Apart from few examples, the use of betaine pyridinium or analog derivatives for a smart manipulation of cation is little explored in the literature.

Since a few years, we have extensively studied the intramolecular charge transfer (ICT) properties of a negative solvatochromic betaine pyridinium,[13] 1-pyridinio-benzimidazolate (Scheme 1) denoted as **PyB**, displaying drastic dipole moment inversion induced by light.[14] In order to get a deep understanding of ICT process at the molecular level, femtosecond transient absorption spectroscopic experiments have been performed and complemented by PCM-TDDFT calculations.[13] An interesting photophysical relaxation scheme has been derived, which involves two distinct ICT excited states, S_1(CT) and S_2(CT). Excitation within the solvatochromic absorption band populates the S_2(CT) state, which leads to partial charge transfer from the betaine phenylene to the pyridinium ring. Then, the S_2(CT) state undergoes ultrafast relaxation to an emissive S_1(E) state in competition with the S_1(CT) state, with a time constant ranging from 300 fs to 20 ps depending on the solvents. The S_2(CT) → S_1(CT) transition involves a charge transfer from the imidazole bridge to the pyridinium ring and thus leads to a further increase of the ICT character. Finally, after few picoseconds, both S_1(CT) and S_1(E) state relaxed with distinct characteristic times. The proper localization of ICT process on the imidazole bridge together with the ability of the latter to attract cations, lead us to undertake the cationic titration of PyB as well as to track the photorelease effect based on ultrafast spectroscopy. Furthermore, within the framework of smart system manipulating cation, we synthesized a novel molecule, aza-crown linked PyB molecule, **PyB-Aza** (Scheme 1), with two possible complexation sites, i.e., the imidazole bridge in competition with the macrocycle. To complete the series, a mono-chelating analog has been synthesized by replacing the aza crown by a dimethyl-amino substituent, **PyB-DiMe** (Scheme 1). We expected that cation will be complexed preferentially by the macrocycle and excitation of the S_2(CT) solvatochromic band will result to the expulsion of the cation, after efficient PCT. In the present work, we found that the imidazole bridge of such betaine pyridinium is finally more efficient to drive for the PCT cation release effect.

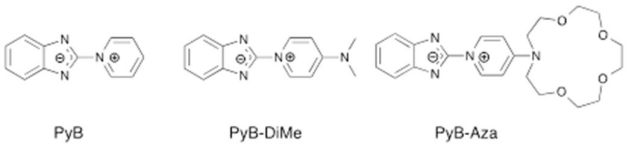

Scheme 1: Betaine pyridinium derivatives PyB-R with R=H, DiMe, Aza-crown

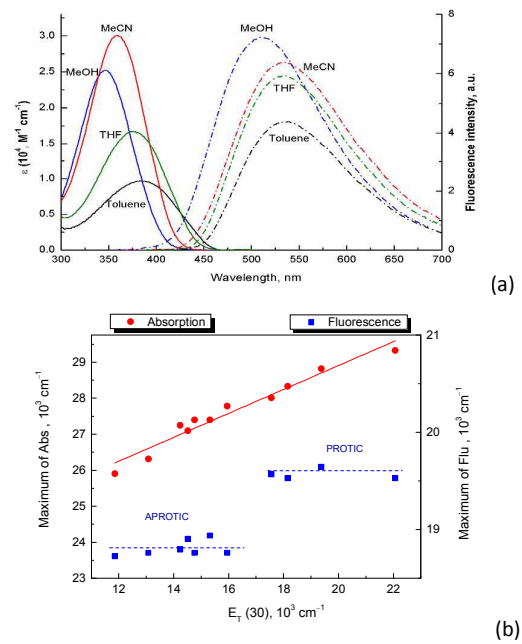

Figure 1.(a) Solvatochromism of PyB-Aza for absorption and fluorescence spectra, the latter being recorded under excitation at maximum absorption wavelengths; direct comparison can be made with Figure 1 of ref 13-a). (b) Absorption/emission solvatochromism plots for PyB-Aza as a function of the E_T(30) polarity index.

Results and discussion

Synthesis of betaine pyridinium derivatives The PyB was synthesized according to the procedure described by Abe et al.[14] The synthesis of PyB-DiMe and PyB-Aza are depicted on Scheme 2. PyB-DiMe was directly obtained from the coupling between 2-chlorobenzimidazole and excessive amount of 4-dimethylaminopyridine (DMAP) in 75% yield.[15] The synthesis of PyB-Aza was performed from the pyridinium derivative **1** (Scheme 1). **1** was achieved by palladium-catalyzed coupling of aza-15-crown-5 with 4-bromopyridine hydrochloride in toluene with a 30% yield.[16] PyB-Aza was then prepared by coupling 2-chlorobenzimidazole and **1** in n-butanol under argon (Ar), followed by deprotonation in concentrated ammonia (NH_3) solution with a 40% yield.[17]

Physical Chemistry Chemical Physics Accepted Manuscript

This journal is © The Royal Society of Chemistry 20xx

Please do not adjust margins

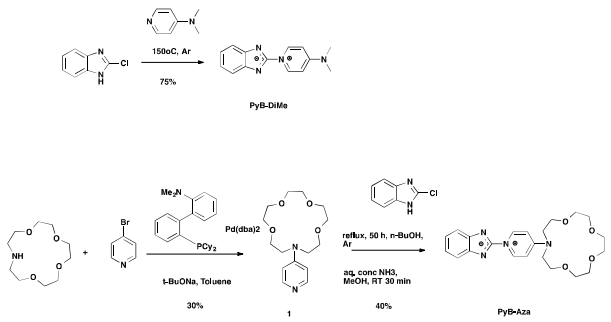

Scheme 2: Synthesis of PyB-DiMe and PyB-Aza

Solvatochromism of PyB-Aza. As explained in the introduction, we are interested to study the ICT properties of betaine pyridinium series PyB-R, PyB being our reference molecule extensively studied in the past.[13] As a matter of fact, one has to ensure that original negative solvatochromic properties reported for PyB are still operative for PyB-Aza despite the crown substitution. Stationary spectra for various solvents are shown in Figure 1a, in which one can easily recognize the same solvent effects for PyB-Aza as for PyB (see Figure 1 of ref 13a): a blue edge absorption band affected by drastic negative solvatochromism while the emission band is slightly affected by the change of the solvent polarity. In the past, absorption and emission spectra of PyB have been assigned through TDDFT calculations as a $S_0 \rightarrow S_2$(FC) transition for absorption and a S_1(opt)$\rightarrow S_0$ transition for emission. The S_2 state arises from a HOMO-1$\rightarrow$LUMO electronic excitation while S_1 corresponds to a HOMO$\rightarrow$LUMO transition. In the present work, applying the same computational strategy for PyB-Aza, we found that the same molecular orbitals (MO) are involved even if energetic inversions are observed; in brief, the absorption band is now assigned has a $S_0 \rightarrow S_1$(FC) transition for substituted PyB derivatives but involves the same MO as the electronic excitation responsible for the absorption process for PyB.

Quantitavely, we have undertaken a complete solvatochromic study in 11 solvents and presented in Figure 1b, results are also gathered together and shown in Table S1. As an evidence, the $E_T(30)$ plot indicates that the ground state (GS) absorption is fully influenced by the electrostatic interacting surrounding medium which contrasts with the non solvatochromic emissive S_1 state. For the latter, apart from the striking partition between protic and aprotic solvent, it is worth to notice that the dipole moment of this emissive state is probably close to zero. As presented in Table S2, Kamlet-Taft correlation coefficients ($\nu_{abs/fluo}=p\pi^*+a\alpha+b\beta$ with the usual meaning; see ref 13b) of PyB-Aza were determined from absorption and emission solvatochromic data. In the case of absorption, coefficient *p* is larger than *a* and *b*, demonstrating that electrostatic interaction dominates the solvatochromism even if the specific hydrogen bonding interaction is not negligible. In the case of emission, *p* is almost negligible when compared with *a* and *b*, meaning that excited state of PyB-Aza is insensitive towards solvent polarity but mainly controlled by the hydrogen bonding interaction which is easily located on the imidazole part of the molecule. Moreover, the ratio a/b are almost the same in the ground state and in the excited state, which might indicate that the same molecular groups are involved in the absorption and emission process. As we have demonstrated for PyB and this is even more pronounced for PyB-Aza that we are dealing with two kinds of singlet state: S_1(CT) related with strong solvatochromic absorption band and S_1(E) related with non solvatochromic emission band.

	Absorption λ_{max}(nm)				Fluorescence λ_{max}(nm)		Complexation constant Log K	
	Ligand		Complex		Ligand	Complex		
	Exp.	Calc.	Exp.	Calc.	Exp.	Exp.	Exp.	Calc.
PyB	393	404	339	387	693	570	3.4 ± 0.1	3.5
PyB-DiMe	356	355	331	330	539	450	6.6±0.1	4.5
PyB-Aza	359	360	335	335	534	450	6.8±0.1	6.4

Table 1 Photophysical data of PyB, PyB-DiMe and PyB-Aza and their 1:1 complex with Ca^{2+} and the binding constants from spectral titrations; corresponding TDDFT results are included (see text for details).

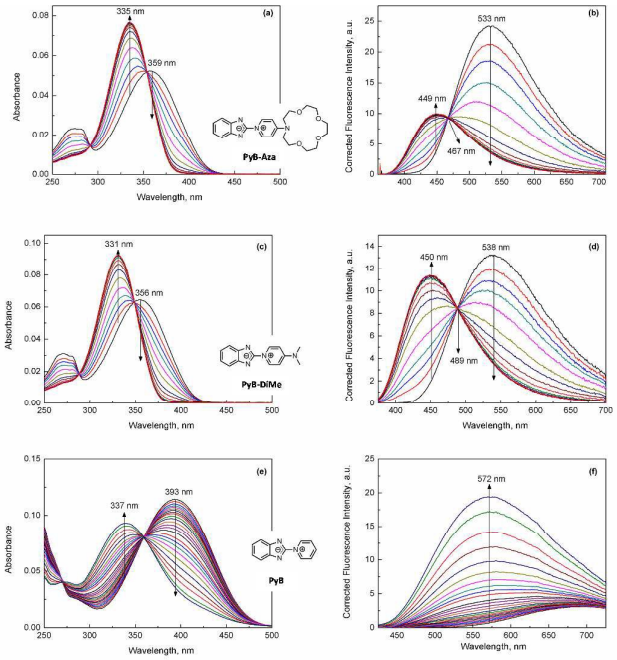

Figure 2. Absorption (a, c, e) and fluorescence (b, d, f) spectra of PyB, PyB-DiMe and PyB-aza) in the presence of increasing concentrations of Ca^{2+} in MeCN; (a, b) [PyB-aza] = 2.5 µM, λ_{ex} = 359 nm; (c, d) [PyB-DiMe] = 2.5 µM, λ_{ex} = 354 nm; (e, f) [PyB] = 10 µM, λ_{ex} = 393 nm.

Cation complexation of PyB-Aza. Solvatochromism being established, we are now concerned with the cation complexation abilities of PyB-Aza where, two chelating groups are in competition i.e., the imidazole bridge vs the crown-ether cavity. To properly undertake such study, the compound PyB-DiMe will be helpful. In the Figure 2 and Table 1, we reported the changes observed in acetonitrile (MeCN) solution containing the three probes upon addition of Ca^{2+} salt (perchlorate) for both absorption and emission. With the addition of Ca^{2+} in the solution of PyB-Aza, gradual decrease in the absorption maximum at 359 nm is observed, concomitantly with the appearance of a new peak at 335 nm. A well-defined isosbestic point at 353 nm indicates the interconversion between the free ligand and the complex during the titration. Blue shift is also observed for fluorescence spectra from 533 nm to 449 nm, with a clear isoemissive point at 467 nm indicating only two emissive species in the solution. As seen in Figure S1, the fluorescence spectra reach a plateau after the introduction of 1 equivalent of Ca^{2+} to the solution of PyB-Aza, demonstrating that the stoichiometry of the complex is 1:1. Global analysis of the whole absorption and emission spectra reveals the formation of 1:1, metal:ligand (M:L) complex and the stability constant was found to be 6.8±0.1 .

Physical Chemistry Chemical Physics Accepted Manuscript

Please do not adjust margins

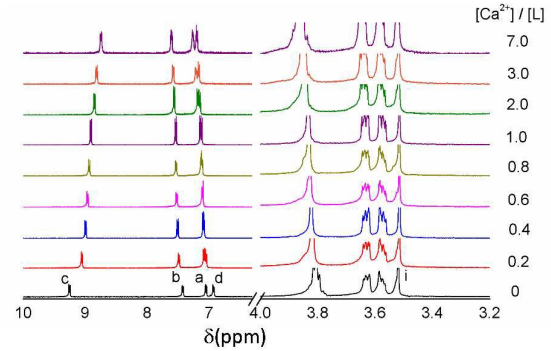

Figure 4. ^{1}H-NMR spectra of PyB-Aza in presence of different concentrations of $Ca(ClO_4)_2$ in CD_3CN.

Before going further into the discussion, the questions about the cation selectivity has to be raised. In the Figure S3, normalized emission intensity for PyB-Aza upon addition of Li^+, Na^+, K^+, Ca^{2+}, Ba^{2+} and Sr^{2+} ions are displayed showing a preferential complexation effect for Ca^{2+} ions. Furthermore, we plot on Figure 3 the polarity parameter $E_T(30)$ as a function of the charge density giving an evidence for the Coulombic nature of the cation-betaine interaction.

Where is the cation located in PyB-Aza? There are two potential binding sites for metal cations in PyB-Aza: benzimidazole moiety and aza-15-crown-5 moiety. In order to get insight into the binding process, ^{1}H NMR titration of PyB-Aza with Ca^{2+} was carried out in CD_3CN. As shown in Figure 4, upon complexation with Ca^{2+}, proton H_c exhibits a remarkable up-field shift, while H_d shows a down-field shift. Protons of H_a and H_b also exhibit a slight down-field shift as compared with H_d. However, it is surprising to find that the addition of Ca^{2+} almost does not affect the chemical shifts of aza-15-crown-5 moiety, which has been widely reported to bind strongly with metal ions.[18] Anyhow, in our case the ^{1}H NMR titration demonstrates that Ca^{2+} strongly binds to imidazole moiety rather than aza-15-crown-5 cavity. Indeed, the up-field shift of the proton H_c could be explained by the disappearance of the electrostatic interaction between H_c and imidazole nitrogen which probably results in a twist of the molecule as shown in the Scheme 3. The slight down-field shift of protons H_a and H_b are logically affected by the presence of the interacting cation.

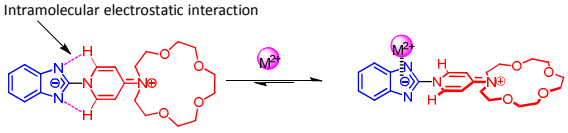

Scheme 3: PyB-Aza interacting with metallic cation.

In order to verify the proposed binding mechanism, similar Ca^{2+} titration were carried out on PyB-DiMe as shown in Figure 1 and Table 1 under identical conditions. Upon addition of increasing concentrations of Ca^{2+}, blue shifts of both the absorption band from 356 nm to 331 nm and the emission band from 538 nm to 450 nm

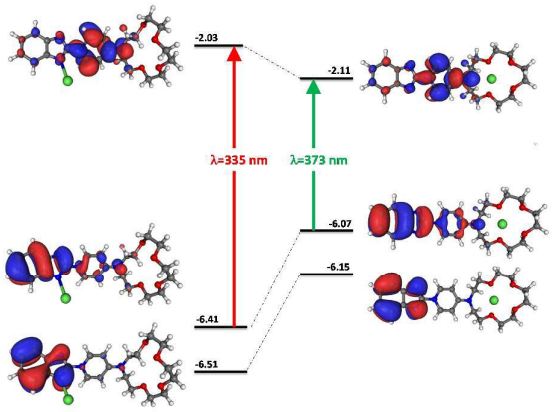

Figure 5. TDDFT calculations BetAza and Ca^{2+} according to lateral (left) or inside crown-ether (right) complexation.

are observed. The clear isosbestic point at 348 nm and the isoemissive point at 489 nm demonstrate the equilibrium between free ligand and complex during the titration. The complexing constant was determined to be 6.63±0.06. All these similarities between PyB-Aza and PyB-DiMe definitively exclude the possibility for cations to be trapped inside the aza-crown cavity. As a matter of fact, the spectral response of PyB to Ca^{2+} addition was also followed in MeCN in order to investigate the effect of amino group appended to pyridinium moiety on the complexation properties induced by the imidazole bridge (Figure 1 and Table 1). The successive addition of Ca^{2+} induces one more time the similar blue shift for both the absorption band from 393 nm to 337 nm and the emission band from 693 nm to 570 nm with Log K = 3.39 a much lower value as compare to PyB-Aza and PyB-DiMe. In conclusion, due to similar spectral changes upon Ca^{2+} addition for the three molecules, it seems reasonable to describe the 1:1 complex as a Ca^{2+} ion interacting electrostatically with the imidazole bridge of the betaine units. In addition, the several orders of magnitude between PyB and the substituted analogs complexation constant can be rationalized in term of donating effect from the azo-dimethyl group enhancing the minus charges located on the imidazole strengthening the attraction upon the cation.

Our computational strategy gives support to experimental findings and confirms the presence of the lateral interaction between the cation and the imidazole bridge rather than complexation inside the macrocycle. As shown in Figure 5, for PyB-Aza , the two systems, (i) the cation inside the crown and (ii) the cation in interaction with the imidazole group, have been determined and the results are displayed for these two systems in Figure 3 as well as an energetic MO diagram with vertical

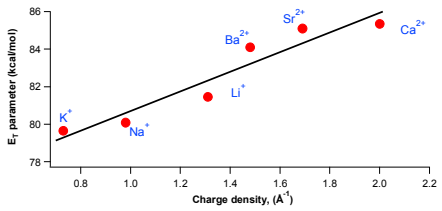

Figure 3. E_T (30) Parameter deduced from absorption spectra after addition of metallic salt (see Figure S2) function of cationic charge density.

This journal is © The Royal Society of Chemistry 20xx

Physical Chemistry Chemical Physics Accepted Manuscript

Please do not adjust margins

transitions determined by TDDFT. The maximum absorption wavelength calculated for the structure corresponding to Ca^{2+} inside the crown is 373 nm in MeCN whereas this wavelength reaches 335 nm for the ion in interaction with the imidazole bridge. The latter structure thus reproduces remarkably and unambiguously the experimental maximum of the absorption at 335 nm. Furthermore, as shown in Table 1, theoretical calculations of log K obtained for the three PyB derivatives with Ca^{2+} bound to the benzimidazole moiety, reproduce remarkably well the experimental values which also confirm the cation complexation site.

Surviving complex upon light excitation: case of PyB? At this point, for the three PyB-R molecules, we obtained strong evidences for an halochromic effect explained by the existence of a (1:1) M:L complex between the imidazole bridge and the cation. Analysis of emission spectra upon salt addition seems to indicate that static quenching occurred rather than dynamic one. With the help of ultrafast absorption spectroscopy, we will now investigate the complex photochemistry after light excitation: will light destabilize the complex or not?

First of all, inspection of PyB transient data, with or without cation, will be the backbones of this study since we have already characterized the post-excitation mechanisms of this molecule in previous articles.[13] In short, its photophysics was discussed in terms of two distinct CT states (S_1 and S_2) and a photophysical scheme was proposed: in parallel to the ultrafast production of the emissive S_1(E) state, an ultrafast ICT process occurs from the initially populated S_2(CT) state to a new charge transfer S_1(CT) state, reaction ranging from 300 fs to 12 ps depending on the solvent. The S_2(CT) → S_1(CT) reaction, was clearly identified by transient spectroscopy with two excited states absorption (ESA) bands evolving in the opposite direction separated with a clear isosbestic point in between. We now present the transient data for PyB in Figure 6a with new experimental conditions (320 nm laser excitation) while the effect of adding Ca^{2+} is presented in Figure 6b according to three distinct temporal windows. Just after excitation ([0-0.5 ps] temporal window), one observes the simultaneous growth of two bands: i) the stimulated emission (SE) negative band coming from S_1(E) state and easily recognized as the negative mirror of the emission band of the free ligand peaking around 690 nm noticed band E_1 (see red curve lower panel); ii) an ESA band attributed to S_2(CT). Both states originate from the relaxation of the S_2 Franck-Condon (FC) state occurring with a $\tau_1 \approx 100$ fs characteristic time. All characteristic times are gathered together in Table 2. Then, the ICT reaction $S_2(CT) \rightarrow S_1(CT)$ proceeds ([0.6-2ps] temporal window) with typical isosbestic point and $\tau_2 \approx 400$ fs characteristic time. Finally, within the [4-600 ps] temporal window, all transient bands vanish with a bi-exponential decay; the shorter time τ_3=7 ps is attributed to S_1(CT) decay via internal conversion (IC) while the longer time τ_4=140 ps is attributed to S_1(E) decay via emission and IC.

The addition of Ca^{2+} changes drastically the photophysics of PyB paralleling the shift of stationary emission signals, band E_2 (with cation) and band E_1 (without cation) being separated for more than 150 nm. Indeed between 0 and 0.25 ps one notice the rise of a new negative SE band i.e., SE_2 peaking at 500 nm concomitantly with a new ESA band near 630 nm (see Figure 6b). Of course, one can expects the PyB-Ca^{2+} complex to emit light after laser excitation

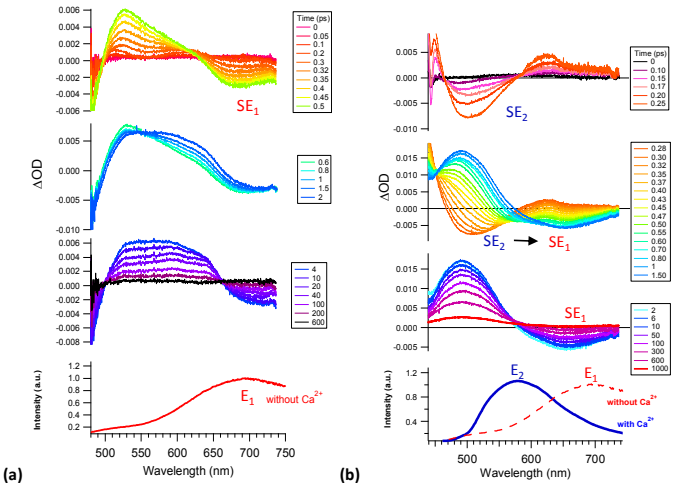

Figure 6 (a) Femtosecond transient absorption spectra of 50 µM of PyB in MeCN following laser excitation at 320 nm, for three temporal windows b) similar data with additional 40 eq. of Ca^{2+} salt in the solution; Lower panels refer to stationary emission spectra for the solution before and afer addition of salt.

which allows to assign safely this negative band as the SE of S_1(E/Ca^{2+}) states but overlapped with its own ESA. Then during [0.28-1.5 ps] temporal window, this SE transient band vanishes in benefit of new ESA peaking at 496 nm together with the negative SE_1 band previously reported. The overall process appears like a drastic shift of negative transient band from blue edge –SE_2 band, to red edge –SE_1 band over more than 150 nm. In accordance with stationary emissions bands E_1 and E_2, we ascertain SE_2 band with S_1(E/Ca^{2+}) due to the complex state while SE_1 band originate from the uncomplexed S_1(E) state. In clear, we assign the transient $SE_2 \rightarrow SE_1$ shift between [0.28-1.5 ps] to the light induced realase of the Ca^{2+} caused by the ICT reaction from benzimidazole moiety to pyridinium moiety, neutralizing the imidazole-Ca^{2+} electrostaic interaction. Global fitting of both rising SE_1 band and vanishing SE_2 band give a characteristic time of 150 fs which is therefore the mean duration for the photorelaese process. Compare to other molecules linked with aza-crown for which the process is reported to occurred within picosecondes regime,[6,9,19] the 150 fs photorelease time of this study is more than one order of

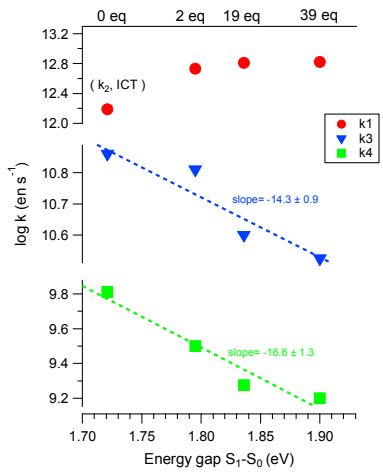

Figure 7 Logarithmic plot of constant rate k_3 and k_4 corresponding to the biexponential decay of the red edge negative transient band (Figure 6a and 6b) function of energy gap S_1-S_0 deduced from stationary emission (Figure 1b).

Physical Chemistry Chemical Physics Accepted Manuscript

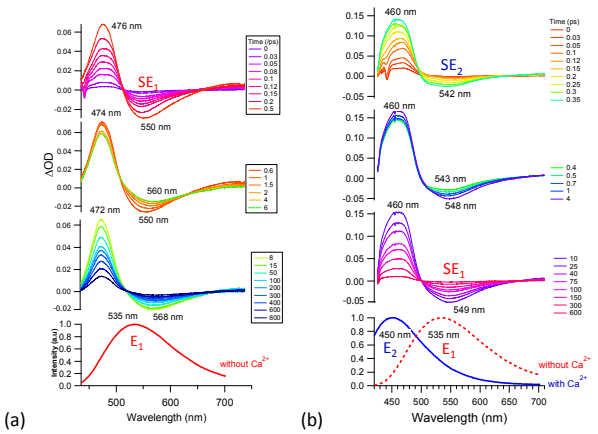

Figure 8 (a) Femtosecond transient absorption spectra of 50 µM of PyB-Aza in MeCN following laser excitation at 320 nm, for three temporal windows b) similar data with additional 100 equivalent of Ca^{2+} salt in the solution; Lower panels refer to stationary emission spectra for the solution before and afer addition of salt.

L L:M	τ_1, ps		τ_2, ps	τ_3, ps	τ_4, ps
	Solvation (FC relaxation)	Cation ejection	ICT S2→S1	decay of S_1(CT)	decay of S_1(E)
PyB	0.10 (2)		0.40 (4)	16 (2)	140 (20)
PyB + Ca^{2+}		0.15 (1)		1.9 (4)	110 (20)
PyB-Aza	0.13 (4)			1.0 (3)	145 (20)
PyB-Aza + Ca^{2+}		0.19 (4)		0.8 (2)	85 (5)
PyB-DiMe	0.10 (2)			0.7 (1)	83 (5)
PyB-DiMe + Ca^{2+}		0.17 (1)		52 (10)	300 (90)

Table 2 Characteristic times deduced from global fitting of transient data for PyB, PyB-DiMe and PyB-Aza;

magnitude faster. Indeed, due to the macrocavity effect, the photorealease mechanism of the crown linked molecules is multisteps and occurred from the picosecond[6,9a,19c,19e,f,20] to the nanosecond regime[19a,b] depending on the cation nature.

Finally, after photoejection, between 2 and 600 ps, the overall transient signal decreases: SE_1 band falls to zero intensity while transient ESA band vanishes, leading to a residual absorption near 490 nm due to a triplet state.[13] A bi-exponential decay is necessary to properly fit the data with two characteristic time τ_3= 1.9 ps and τ_4= 110 ps related to S_1(CT) and to S_1(E) respectively. It is worth to note that the final deexcitation of the singlet states do not drastically depend on the presence or absence of cation which suggest that the Ca^{2+} is probably release into the bulk. Further analysis can be undertaken to support this statement. Indeed, it is worth to consider that even after ejection of the cations out to the first solvation shell, cations are still localized inside the subsequent shells stressing Coulombic interactions for the ground and excited states of PyB. Unlike the photo-ejection process (k_1) both decays with rates k_3 and k_4 are expected to obey the well-known "energy gap law"

$$\log k \propto log k_0 - \frac{1}{RT}\Delta E(S_1 S_0) \quad (1)$$

where $\Delta E(S_1S_0)$ refers to the energy differences between first excited and ground states at a given temperature T , whereas R is the gas constant. In Figure 7, we present the logarithmic plot of k_1 (or k_2 without Ca^{2+}), k_3 and k_4 deduced from global fitting of transient data after addition of 0, 2, 19 and 39 equivalents of Ca^{2+} function of the S_1-S_0 energy gap obtained from the maximum of emission for these respective solutions. As expected, photo-ejection case (first panel) does not depend on calcium concentration while subsequent decays gives evidence that equation 1 is fully satisfied, the slope being close to the expected value of -15.5 eV^{-1}. Closer inspection of characteristic times in Table 2 shows higher value of τ_4 (S_1(E) decay) as compare to τ_3 (S_1(CT) decay) regardless the presence of cation or not. This is consistent with a lack of specific interaction between PyB* and the photo-ejected Ca^{2+} the latter having probably escaped into the bulk. As a partial conclusion, the photophysics of the PyB-Ca^{2+} M:L complex can be summarized by a photorelease of the cation within 150 fs, (PyB-Ca^{2+})* = PyB* + Ca^{2+}, followed by the decay of two S_1 states ranging from 14 to 600 ps but significantly influenced by the presence of cations located in the second solvation sphere.

Photoejection of cation upon PyB-Aza light excitation? In the continuity of PyB analysis, transient data for PyB-Aza in MeCN is presented in Figure 8a and also divided into three temporal windows. Displayed on the first panel (up to 0.6 ps), an initial growth of ESA band peaking at 476 nm is observed with concomitantly growth of SE_1 negative bands with a characteristic time of τ_1=130 fs. Following TDDFT assignments, 320 nm laser excitation falls up to S_1 state and by analogy with the previous case, both native transient bands are straightforwardly related to the S_1(CT) and S_1(E) states populated after S_1 Franck-Condon state deexcitation. Inspecting the second temporal window of Figure 8a), still in comparison with PyB (second panel of Figure 6a), one has to notice the lack of S_2→ S_1 IC spectral signatures which coincides logically with the fact that optically accessible state is S_1 state rather than S_2 (let's say that τ_2 is missing). Finally, on the third temporal window, ESA and SE_1 bands vanished leaving a persisting signal peaking at 470 nm attributed to be the triplet state (see discussion above). As already discussed, the double exponential decay is easily assigned: τ_3~1 ps is the IC S_1(CT)→S_0 while τ_4~140ps represents the decay of S_1(E) state. As shown in Figure S3, results for PyB-DiMe are strictly similar to PyB-Aza, except for the numerical values of the characteristic times τ_1, τ_3 and τ_4 as given in Table 2.

Analysis of transient data for the PyB-Aza-Ca^{2+} complex is a central result of this article because we want to assess if such stable species (logK~7) is still able to release the cation upon light excitation in a similar way as compare to the weak bonded analog PyB-Ca^{2+} (log K~4).

Unlike the previous molecule, the ultrafast photophysics of PyB-Aza-Ca^{2+} complex is less simple to analyse because emissive states without (band E_1 at 535nm) and with cation (band E_2 at 450 nm) are less spaced (85 nm) than in the case of PyB (125 nm). Indeed, ESA and SE band strongly overlap peaking at the same wavelength at about 460 nm. Indeed, on the first two panels, compared to Figure 6b, we cannot distinguish distinctly the drastic shift SE_2→SE_1 due to this strong spectral overlap of positive ESA bands (at 460nm) with the expected negative SE_2 band. Anyhow, until 350 fs, we can notice a small negative band peaking at 542 nm that can be assigned to the foot of SE_2 (negative mirror of band E_2). Then, after

Physical Chemistry Chemical Physics Accepted Manuscript

This journal is © The Royal Society of Chemistry 20xx

Please do not adjust margins

400 fs, the slight red shift of the negative band can be ascribed to the cation photo-release reaction since the 4 ps trace can be assigned to the free ligand SE_1 signal. As seen in Table 2, the characteristic time for such reaction is 190 fs. Finally, after the photorelease, between 2 and 1000 ps (third panel of Figure 8), we propose to assign the double exponential decay as the respective decays of the two singlets, i.e. τ_3=0.8 ps for S_1(CT) and τ_4=85 ps for S_1(E) previously reviewed. Similar results are obtained for PyB-DiMe molecule (see Supporting Information Figure S3) with distinct characteristic times reported in Table 2. Note that any translocation reaction between the imidazole bridge and the macrocycle can be reported for PyB-Aza the Ca^{2+} being probably ejected into the bulk.

Is the Betaine pyridinium an efficient molecular brick for advanced photo-manipulation of cation? Up to now, the most common approach to build cation photorelease systems was to couple an aza-crown cavity with a PCT moiety: after PCT, the heteroatom of the macrocycle is positively charged, resulting in the Coulombic repulsion between the heteroatom and the metal cation initially inside the cavity. However, as nicely evidenced by several groups, the mechanism for the photoejection process is complex with the enrolment of at least one transient intermediate, the so-called loose complex, a kind of pre-dissociated species for which the cation is still weakly interacting with the aza-crown.[9a,19d] The photorealease mechanism of this crown linked molecules are multisteps and occurred from the picosecond[6,9a,19c,19e,f,20] to the nanosecond regime[19a,b] depending on the cation nature. Furthermore, as already emphazised by Kumar et al. that coordination-based open system avails the opportunity to explore efficiently rigid sensory system and appeal of metal ions toward molecular receptors.[8]

Such drawbacks are overpassed with PyB-R series. First of all, the photorelease mechanism is instantaneous avoiding the loose complex formation reported for the aza-crown related molecules. Furthermore, to the best of our knowledge, the ~200 fs is the fastest never reported in the literature. The simplicity of the photo-release process is merely due to the lateral and strong Coulombic interaction engaging only one nitrogen of the imidazole moiety. Furthermore, the PyB-R can be a very efficient chelatant, log K~6-7, and purely stoichiometric because only the 1:1 M:L complex is reported. Clearly, a promising result concerns the modulation of the complexation toward para substitution of the phenyl ring with a donor group. Indeed, for the series R=H, DiMe, Aza-crown the complexation constants vary as log K=3.4, 6.6 and 6.8, respectively. From a photochemical point of view, for the same series, the trend is parallel to the rate of the photorelease process k_1 (Table 2) varying as 150, 170 and 190 fs. Still focusing on the complexation constant, state-of-the-art TDDFT strategy chosen by our group was able to reproduce quantitatively the experimental values.

Conclusions

Based on advanced spectroscopy in combination with TD-DFT calculations, the complexation and photorelease properties of PyB-Aza, PyB-DiMe and PyB on metallic cation has been investigated. In the continuity of our work undertaken in the past for PyB, it has first been found that the photophysics of PyB-Aza is characterized by one strong solvatochromic singlet excited state, S_1(CT), and one non-solvatochromic emissive state S_1(E). Upon metallic salt addition, absorption and emission spectroscopy of the three molecules have clearly revealed that the cation were not trapped on the macrocycle but strongly attracted by negative charges located on the imidazole moiety. The stoichiometry of the complex was (1:1).

Due to the Coulombic nature of the complexation, high charge density cations like Ca^{2+} are especially sensitive to the imidazole attraction. The possibility to tune the complexation strength upon pyridinium moiety substitution has been clearly identified with the series, PyB-R with R= R=H, DiMe and Aza-crown the complexation constant rising from 3.4 to 6.8, i.e. more than three order of magnitudes.

Upon light excitation, an ultrafast one-step photo-release reaction proceeds,

$$PyB\text{-}R{:}Ca^{2+} + h\upsilon \rightarrow PyB\text{-}R^* + Ca^{2+}$$

the remaining ligand excited state being either S_1(CT) or S_1(E). The value of the rate k_1 (~$1/\tau_1$) is parallel to the ground state complexation constant. The lower the log K, the lower the stability of the complex, the higher the photorelease rate k_1. State-of-the-art TDDFT calculations were able to reproduce perfectly the experimental values of complexation constant. Based on the same computational strategy, we were initiating a molecular design campaign to elaborate a smart bio-compatible system enabling the light induced Ca^{2+} translocation from the imidazole moiety to a second chelating site.

Experimental

General

All commercially available reagents were used without further purification. Column chromatography was performed on silicagel 60 (40–60µm). The solvents for column chromatography were used without purification. The reactions carried out under anhydrous conditions are performed under argon (Ar) in glassware previously dried in an oven. All commercially available reagents were used without further purification. NMR spectra were recorded on a JEOL ESC-400 spectrometer in $CDCl_3$ or in CD_3CN solvents. The chemical shift was given in units of parts per million related to TMS or solvent protons as internal reference. Mass spectrometry analyses were performed at IMAGIF/ICSN

1-*N*-Benzimidazolyl-4-dimethylaminopyridiunium: PyB-DiMe: To a schlenk tube 2-chlorobenzimidiaole (0.2 g, 1.32 mmol) and dimethylpyridine (1.6 g, 13.2 mmol) were added. After the reaction mixture was stirred at 150°C for 3 h under Ar, it was cooled down to room temperature followed by the addition of 30 mL H_2O. The precipitate was filtered off and washed with water and ethanol twice to obtain a pure product. (0.27 g, 75%). **^{1}H NMR** (400 MHz, CD_3OD): (d, *J* = 8.2

Physical Chemistry Chemical Physics Accepted Manuscript

Hz, 2H), (dd, *J* = 6.4, 3.2 Hz, 2H), (d, *J* = 7.8 Hz, 2H), (dd, *J* = 6.4, 3.2 Hz, 2H), (s, 6H); **^{13}C NMR** (100 MHz, CD_3OD): 158.3, 154.9, 146.1, 138.9, 121.3, 117.4, 108.6, 48.4 ppm; **HRMS** (ESI) *m/z* calcd for $C_{14}H_{15}N_4$ [M + H^+] 239.1297, found 239.1289.

N-Pyridine-aza-15-crown-5: 1: To a schlenk tube, 4-bromopyridine hydrochloride (0.2 g, 1.0 mmol) aza-15-crown-5 (0.1 g, 0.46 mmol), *t*-BuONa (0.19 g, 2.0 mmol), $Pd(dba)_2$ (21 mg, 0.04 mmol) and 2-dicyclohexylphosphino-2'-(*N,N*-dimethylamino)biphenyl (20 mg, 0.05 mmol) were added. The reaction mixture was stirred at 100°C for 41 h under Ar. Crude product containing some triethyl amine (Et_3N) and aza-15-crown-5 was obtained by column chromatography on silica gel (elute: MeOH/DCM/Et_3N = 5:95:0.5) (40 mg, 30%).**^{1}H NMR** (400 MHz, $CDCl_3$): (d, J = 5.5 Hz, 2H), (d, J = 5.0, 2H), (m, 20H);[21]

1-(1-*N*-Benzimidazolylpyridiunium)-aza-15-crown-5: PyB-aza: Compound **1** (0.17 g, 0.57 mmol) and 2-chlorobenzimidiazole (0.13 g, 0.86 mmol) were dissolved in dry *n*-BuOH (3 mL) were stirred at 110°C for 50 h under Ar. The solvent was evaporated and the residual was redissolved in MeOH (2 mL) followed by the addition of concentrated aqueous NH_3 (33%, 1 mL) and stirred at room temperature for 30 min. The solvent was evaporated and the crude product was separated by column chromatography (elute: MeOH/DCM/Et_3N = 2:95:1) to obtain a viscous solid which was dissolved in diluted aqueous NH_3 (10%) and extracted with $CHCl_3$. The organic layer was dried over $MgSO_4$ and evaporated to obtain the yellow solid (100 mg, 40%).**^{1}H NMR** (400 MHz, $CDCl_3$): (d, *J* = 7.8 Hz, 2H), (dd, *J* = 6.0, 3.2 Hz, 2H), (dd, *J* = 6.0, 3.2 Hz, 2H), (d, *J* = 7.8 Hz, 2H (t, *J* = 5.5 Hz, 4H), (m, 12H), (s, 4H); **^{13}C NMR** (100 MHz, $CDCl_3$): 156.2, 154.1, 146.0, 137.8, 120.0, 117.0, 107.4, 72.3, 70.6, 70.0, 68.1, 53.8 ppm; **HRMS (ESI)** *m/z* calcd for $C_{22}H_{29}N_4O_4$ [M + H^+] 413.2189, found 413.2179.

Spectroscopic technics. All stationary absorption and fluorescence spectra were recorded using double beam CARY 5000 and FluoroMax 3 spectrometers, respectively. The spectral resolution is typically 2 nm in both experiments. Emission spectra were corrected for the lamp and detector response. Measurements were performed at ambient temperature using 1 cm quartz cells with about 10^{-5} M solutions, keeping the maximum absorbance at less than 0.1 in order to avoid any significant reabsorption effects. Complexation constants were determined by global analysis of the evolution of all absorption and/or emission spectra by using the Specfit Global Analysis System V3.0 for 32-bit Windows system. This software uses singular value decomposition and nonlinear regression modelling by the Levenberg–Marquardt method.[22]

Transient absorption experimental set up (solution). The femtosecond transient absorption set up had already been described elsewhere.[23] Briefly, a 1-kHz Ti:sapphire laser system (coherent oscillator and a BM Industries regenerative amplifier) delivered 100 fs (0.8 mJ) pulses at 800 nm. Pump pulses were set at 350 nm by using a Palittra NOPA, while probe pulses (white light continuum) were generated by focusing the fundamental beam in a CaF_2 rotating plate. The transient absorption measurements covered a 400-750 nm spectral range and a 0-3 ns temporal range. Sample solutions (about 10^{-4} M) were circulating in a flow cell equipped with 100 µm thick CaF_2 windows and characterized by a 1 mm optical path length. The laser cross-correlation time has been evaluated to be about 200 fs and 300 fs at 390 nm and 266 nm, respectively.[23] The characteristic times deduced from kinetics were obtained by fitting the GVD corrected data using (procedure proposed by Nakayama *et al.*[24]) with the result of a multi-exponential function convolved with a Gaussian pulse which approximates the pump-probe correlation function. Within this approach, global fitting were systematically performed taking into account simultaneously four or five relevant wavelengths.

Theoretical calculations. To calculate the absorption and fluorescence properties, we used density functional theory (DFT) and time-dependent density functional theory (TDDFT) formalisms according to the three-step methodology: i) the ground state (GS) and excited states (ES) geometries of each structure were optimized without any symmetry constraint in the equilibrium limit using the linear-response (LR) polarized continuum model (PCM);[25] ii) the vibrational spectra were computed at the same level of theory to check that the optimized structures correspond to true minima on the potential energy surface; iii) the vertical transition energies to the excited states were computed with TD-DFT within the PCM scheme, relying on the state-specific (SS) approximation in its non-equilibrium limit.[26] All these calculations were performed using Gaussian 09 package[27] at the PBE0/6-31+G(d) level, a strategy previously used for PyB.[13a,13c]

To calculate the complexation energy and the complexation constant (log K), we used the thermodynamic cycle presented in Figure S4. The change of Gibbs free energy of reaction between the ligand and the ion ΔG^0_{sol} corresponds to the sum of the gas-phase Gibbs free energy of reaction ΔG^0_{gas} and the change in solvation energy, ΔG^0_{solv}:

$$\Delta G^0_{sol} = \Delta G^0_{gas} + \Delta G^0_{solv}$$

which leads to

$$\Delta G^0_{sol} = \Delta G^0_{gas} + G^0_{solv}(complex) - G^0_{solv}(ligand) - G^0_{solv}(Ca^{2+})$$

with

$$\Delta G^0_{gas} = G^0_{gas}(complex) - G^0_{gas}(ligand) - G^0_{gas}(Ca^{2+})$$

The standard enthalpy and Gibbs free energy at 298.15 K in gas phase were calculated by adding the thermal correction obtained by frequency analysis to the DFT calculation (zero-point energies corrections, ZPE, were considered). The interaction energies were corrected for basis set superposition error (BSSE) using the counterpoise method. [28] To calculate the solvation energy, we have used the PCM model.

Acknowledgements

Chevreul institute (FR 2638), Ministère de l'Enseignement Supérieur et de la Recherche, Région Nord – Pas de Calais and FEDER are acknowledged for supporting and funding this work.

Notes and references

1 (1) Carafoli, E. *Annual Review of Biochemistry* **1987**, *56*, 395.

This journal is © The Royal Society of Chemistry 20xx

Please do not adjust margins

Physical Chemistry Chemical Physics Accepted Manuscript

2 (2) Brieke, C.; Rohrbach, F.; Gottschalk, A.; Mayer, G.; Heckel, A. *Angew Chem Int Ed Engl* **2012**, *51*, 8446.

3 (3) (a) Bort, G.; Gallavardin, T.; Ogden, D.; Dalko, P. I. *Angew Chem Int Ed Engl* **2013**, *52*, 4526(b) Korzycka, K. A.; Bennett, P. M.; Cueto-Diaz, E. J.; Wicks, G.; Drobizhev, M.; Blanchard-Desce, M.; Rebane, A.; Anderson, H. L. *Chem. Sci.* **2015**, *6*, 2419.

4 (4) Momotake, A.; Lindegger, N.; Niggli, E.; Barsotti, R. J.; Ellis-Davies, G. C. *Nature methods* **2006**, *3*, 35.

5 (5) (a) Lewis, J. D.; Moore, J. N. *Chemical Communications* **2003**, 2858(b) Lewis, J. D.; Perutz, R. N.; Moore, J. N. *Journal of Physical Chemistry A* **2004**, *108*, 9037.

6 (6) Douhal, A.; Roshal, A. D.; Organero, J. A. *Chemical Physics Letters* **2003**, *381*, 519.

7 (7) Vantomme, G.; Lehn, J. M. *Angew Chem Int Ed Engl* **2013**, *52*, 3940.

8 (8) Kumar, A.; Chhatwal, M.; Gupta, T. *Tetrahedron Letters* **2012**, *53*, 5691.

9 (9) (a) Ley, C.; Lacombat, F.; Plaza, P.; Martin, M. M.; Leray, I.; Valeur, B. *Chemphyschem* **2009**, *10*, 276(b) Plaza, P.; Leray, I.; Changenet-Barret, P.; Martin, M. M.; Valeur, B. *Chemphyschem* **2002**, *3*, 668.

10 (10) (a) Valeur, B.; Leray, I.; Zhao, L. Y.; Souchon, V.; Metivier, R.; Plaza, P.; Ley, C.; Lacombat, F.; Martin, M. M. *Chemphyschem* **2010**, *11*, 2416(b) Dozova, N.; Kumar, R.; Pradhan, T.; Lacombat, F.; Valeur, B.; Kim, J. S.; Plaza, P. *Chemical Communications* **2015**, *51*, 14859.

11 (11) Reichardt, C. *Chemical Society Reviews* **1992**, *21*, 147.

12 (12) Reichardt, C.; Asharin; Fard, S.; Schäfer, G. *Chemische Berichte* **1993**, *126*, 143.

13 (13) (a) Aloise, S.; Pawlowska, Z.; Ruckebusch, C.; Sliwa, M.; Dubois, J.; Poizat, O.; Buntinx, G.; Perrier, A.; Maurel, F.; Jacques, P.; Malval, J. P.; Poisson, L.; Piani, G.; Abe, J. *Physical Chemistry Chemical Physics* **2012**, *14*, 1945(b) Pawlowska, Z.; Lietard, A.; Aloise, S.; Sliwa, M.; Idrissi, A.; Poizat, O.; Buntinx, G.; Delbaere, S.; Perrier, A.; Maurel, F.; Jacques, P.; Abe, J. *Physical Chemistry Chemical Physics* **2011**, *13*, 13185(c) Perrier, A.; Aloise, S.; Pawlowska, Z.; Sliwa, M.; Maurel, F.; Abe, J. *Chemical Physics Letters* **2011**, *515*, 42.

14 (14) Abe, J.; Shirai, Y.; Nemoto, N.; Miyata, F.; Nagase, Y. *J Phys Chem B* **1997**, *101*, 576.

15 (15) Alcalde, E.; Dinares, I.; Elguero, J.; Fayet, J. P.; Vertut, M. C.; Miravitlles, C.; Molins, E. *The Journal of Organic Chemistry* **1987**, *52*, 5009.

16 (16) Chi, K. W.; Addicott, C.; Stang, P. J. *J Org Chem* **2004**, *69*, 2910.

17 (17) Nemoto, N.; Abe, J.; Miyata, F.; Shirai, Y.; Nagase, Y. *J Mater Chem* **1998**, *8*, 1193.

18 (18) (a) Lewis, J. D.; Moore, J. N. *Dalton Transactions* **2004**, 1376(b) Yoshida, K.; Mori, T.; Watanabe, S.; Kawai, H.; Nagamura, T. *Journal of the Chemical Society-Perkin Transactions 2* **1999**, 393(c) Letard, J. F.; Lapouyade, R.; Rettig, W. *Pure and Applied Chemistry* **1993**, *65*, 1705.

19 (19) (a) Lednev, I. K.; Ye, T.-Q.; Hester, R. E.; Moore, J. N. *The Journal of Physical Chemistry A* **1997**, *101*, 4966(b) Lednev, I. K.; Hester, R. E.; Moore, J. N. *The Journal of Physical Chemistry A* **1997**, *101*, 7371(c) Martin, M. M.; Plaza, P.; Meyer, Y. H.; Badaoui, F.; Bourson, J.; Lefevre, J. P.; Valeur, B. *Journal of Physical Chemistry* **1996**, *100*, 6879(d) Létard, J. F.; Delmond, S.; Lapouyade, R.; Braun, D.; Rettig, W.; Kreissler, M. *Recueil des Travaux Chimiques des Pays-Bas* **1995**, *114*, 517(e) Martin, M. M.; Plaza, P.; Meyer, Y. H.; Begin, L.; Bourson, J.; Valeur, B. *Journal of fluorescence* **1994**, *4*(f) Martin, M. M.; Plaza, P.; Hung, N. D.; Meyer, Y. H.; Bourson, J.; Valeur, B. *Chemical Physics Letters* **1993**, *202*, 425.

20 (20) Mathevet, R.; Jonusauskas, G.; Rulliere, C.; Letard, J.-F.; Lapouyade, R. *The Journal of Physical Chemistry* **1995**, *99*, 15709.

21 (21) Kotsuki, H.; Sakai, H.; Shinohara, T. *Synlett* **2000**, *2000*, 116.

22 (22) Gampp, H.; Maeder, M.; Meyer, C. J.; Zuberbühler, A. D. *Talanta* **1985**, *32*, 95.

23 (23) (a) Buntinx, G.; Naskrecki, R.; Poizat, O. *Journal of Physical Chemistry* **1996**, *100*, 19380(b) Moine, B.; Rehault, J.; Aloise, S.; Micheau, J. C.; Moustrou, C.; Samat, A.; Poizat, O.; Buntinx, G. *Journal of Physical Chemistry A* **2008**, *112*, 4719.

24 (24) Nakayama, T.; Amijima, Y.; Ibuki, K.; Hamanoue, K. *Review of Scientific Instruments* **1997**, *68*, 4364.

25 (25) Tomasi, J.; Mennucci, B.; Cammi, R. *Chemical Reviews* **2005**, *105*, 2999.

26 (26) Mennucci, B. *The Journal of Physical Chemistry Letters* **2010**, *1*, 1666.

27 (27) Gaussian 09, R. A., Frisch, M. J.; Trucks, G. W.; Schlegel, H. B.; Scuseria, G. E.; Robb, M. A.; Cheeseman, J. R.; Scalmani, G.; Barone, V.; Mennucci, B.; Petersson, G. A.; Nakatsuji, H.; Caricato, M.; Li, X.; Hratchian, H. P.; Izmaylov, A. F.; Bloino, J.; Zheng, G.; Sonnenberg, J. L.; Hada, M.; Ehara, M.; Toyota, K.; Fukuda, R.; Hasegawa, J.; Ishida, M.; Nakajima, T.; Honda, Y.; Kitao, O.; Nakai, H.; Vreven, T.; Montgomery, Jr., J. A.; Peralta, J. E.; Ogliaro, F.; Bearpark, M.; Heyd, J. J.; Brothers, E.; Kudin, K. N.; Staroverov, V. N.; Kobayashi, R.; Normand, J.; Raghavachari, K.; Rendell, A.; Burant, J. C.; Iyengar, S. S.; Tomasi, J.; Cossi, M.; Rega, N.; Millam, N. J.; Klene, M.; Knox, J. E.; Cross, J. B.; Bakken, V.; Adamo, C.; Jaramillo, J.; Gomperts, R.; Stratmann, R. E.; Yazyev, O.; Austin, A. J.; Cammi, R.; Pomelli, C.; Ochterski, J. W.; Martin, R. L.; Morokuma, K.; Zakrzewski, V. G.; Voth, G. A.; Salvador, P.; Dannenberg, J. J.; Dapprich, S.; Daniels, A. D.; Farkas, Ö.; Foresman, J. B.; Ortiz, J. V.; Cioslowski, J.; Fox, D. J. Gaussian, Inc., Wallingford CT **2009**.

28 (28) Boys, S. F.; Bernardi, F. *Molecular Physics* **1970**, *19*, 553.

29

Physical Chemistry Chemical Physics Accepted Manuscript